ARTICLE OPEN

Check for updates

Correlations of blood and brain NMR metabolomics with Alzheimer's disease mouse models

Franz Knörnschild[1,7], Ella J. Zhang[1,7], Rajshree Ghosh Biswas[1,7], Marta Kobus[1], Jiashang Chen[1], Jonathan X. Zhou[1], Angela Rao[1], Joseph Sun[1], Xiaoyu Wang[1], Wei Li[2], Isabella H. Muti[1], Piet Habbel[3], Johannes Nowak[4,5], Zhongcong Xie[2], Yiying Zhang[2]✉ and Leo L. Cheng[1,6]✉

Alzheimer's disease (AD) is a complex, progressive neurodegenerative disorder, impacting millions of geriatric patients globally. Unfortunately, AD can only be diagnosed post-mortem, through the analysis of autopsied brain tissue in human patients. This renders early detection and countering disease progression difficult. As AD progresses, the metabolomic profile of the brain and other organs can change. These alterations can be detected in peripheral systems (i.e., blood) such that biomarkers of the disease can be identified and monitored with minimal invasion. In this work, High-Resolution Magic Angle Spinning (HRMAS) Nuclear Magnetic Resonance (NMR) spectroscopy is used to correlate biochemical changes in mouse brain tissues, from the cortex and hippocampus, with blood plasma. Ten micrograms of each brain tissue and ten microliters of blood plasma were obtained from 5XFAD Tg AD mice models ($n = 15$, 8 female, 7 male) and female C57/BL6 wild-type mice ($n = 8$). Spectral regions-of-interest (ROI, $n = 51$) were identified, and 121 potential metabolites were assigned using the Human Metabolome Database and tabulated according to their trends (increase/decrease, false discovery rate significance). This work identified several metabolites that impact glucose oxidation (lactic acid, pyruvate, glucose-6-phosphate), allude to oxidative stress resulting in brain dysfunction (L-cysteine, galactitol, propionic acid), as well as those interacting with other neural pathways (taurine, dimethylamine). This work also suggests correlated metabolomic changes within blood plasma, proposing an avenue for biomarker detection, ideally leading to improved patient diagnosis and prognosis in the future.

Translational Psychiatry (2025)15:87 ; https://doi.org/10.1038/s41398-025-03293-8

INTRODUCTION

Alzheimer's disease (AD) is one of the most complex neurodegenerative disorders, impacting over 6 million Americans as estimated by the National Institute of Aging [1, 2]. In the past 20 years, reported deaths from AD have increased by 145%, making it the fifth-leading cause of death for geriatric patients in the U.S. in 2023 [1, 2]. As AD is characterized by a broad variety of clinical impairments in multiple cognitive, functional, and behavioral domains, individuals suffering from AD-dementia experience a gradual decline in neurocognitive abilities, leading to an increased need for support that also drastically impacts the lives of their caretakers [3]. With an ever-growing number of AD cases, a minimally invasive technique for detection of this deleterious disease is required.

AD is commonly characterized by the deposition of amyloid plaques, which can be composed of extracellular amyloid-β (Aβ) protein, neurofibrillary tangles, and intracellular tau protein, into brain structures critical for memory and cognition [4]. Due to this proteinopathy, AD brains experience a dramatic loss of neuronal and astrocytic function, alteration of synaptic connections, and cell death [4]. However, recent studies have revealed deficiencies in brain metabolism and mitochondrial bioenergetics in numerous neurodegenerative disorders, including AD, suggesting that AD should be considered a metabolic disease [5]. Despite major advances in imaging techniques and biomarker identification, AD relies on evaluations of clinical parameters rather than examinations of the disease itself. As there are no non-invasive methods of diagnosing and characterizing AD during a patient's lifetime, a definitive AD diagnosis can only be achieved at autopsy, based on brain tissue pathology. This limits the development of potential strategies for countering disease progression [6, 7], as well as discoveries of AD-associated metabolomics markers that may be evaluated through measurements of peripheral systems, such as blood.

As AD develops and progresses, the overall metabolic status of the brain and other organs may alter in AD patients, transitioning from normal homeostasis of healthy individuals to states likely preceding the formation of AD pathologies. Evaluations and quantifications of these metabolic changes in terms of AD metabolomics may assist in AD detection and diagnosis. Although human pathological materials, such as brain tissues from autopsied AD patients, can be used to attempt discoveries of

[1]Departments of Radiology and Pathology, Massachusetts General Hospital, Harvard Medical School, Boston, MA, USA. [2]Department of Anesthesia, Massachusetts General Hospital, Harvard Medical School, Boston, MA, USA. [3]Charité – Universitätsmedizin Berlin, Berlin, Germany. [4]SRH Poliklinik Gera GmbH, Radiology Gotha, Gotha, Germany. [5]SRH University of Applied Health Sciences, Gera, Germany. [6]Department of Environmental Health, Harvard T.H. Chan School of Public Health, Boston, MA, USA. [7]These authors contributed equally: Franz Knörnschild, Ella J. Zhang, Rajshree Ghosh Biswas. ✉email: yzhang37@mgh.harvard.edu; leocheng@hsph.harvard.edu

Received: 30 May 2024 Revised: 14 December 2024 Accepted: 19 February 2025
Published online: 18 March 2025

disease-related metabolic alterations, these cellular metabolites may vary due to differing tissue preservation conditions after death, thereby failing to reflect their state in vivo. To overcome these postmortem metabolic alterations and degradations, studies of experimental animal models under controlled environments and standardized protocols have been developed [8, 9], where both brain and blood metabolomics can be measured simultaneously. Current practices (also being developed in clinical trials) of diagnosing AD with blood-based biomarkers use a targeted approach, where assays detect plasma Aβ42/Aβ40 or p-tau levels [10]. Here we utilize a non-targeted metabolomic approach to identify metabolites associated with AD in blood plasma, which can provide information as to specific biochemical pathways being impacted and provide complementary information to targeted assays. Correlating biomarkers from blood to understand pathological states in brain tissue can provide an avenue for improving disease detection, with minimal invasion, ideally leading to better patient diagnosis and prognosis in the future.

We have previously demonstrated the ability of high-resolution magic angle spinning (HRMAS) NMR to differentiate AD and wild-type (WT) mice by comparing brain metabolomic alterations observed in hippocampal and cortical brain regions [11]. Briefly, HRMAS NMR allows for the detection of metabolites within gel-like and tissue samples with minimal sample preparation, where spinning samples at the magic angle (54.7°) narrows the spectral lineshape in complex heterogenous samples [12]. Due to their significant role in learning, memory, and behavioral function, both cortex and hippocampus tissue were evaluated and monitored for metabolomic changes in mice with and without AD. In this study, we present evidence correlating metabolomic changes (exhibiting similar or opposite trends) in brain tissue (cortex, hippocampus) and those in blood measured from AD mouse models with HRMAS NMR.

MATERIALS & METHODS

Ethics approval and consent to participate

All methods performed in this study were approved by the MGH Institutional Animal Care and Use Committee (IACUC), permit number 2006N00CI0219 in accordance with the institutional guidelines and regulations.

Animal models

In this study, we used 5XFAD Tg Alzheimer's disease (AD) mice at 14 months of age ($n = 15$, 8 female, 7 male) and female C57/BL6 wild-type (WT) mice at 12 months of age ($n = 8$). Over the age of 12 months, 5XFAD mice generally represent a late-stage model of AD in humans, corresponding to advanced AD pathology including extensive amyloid plaque accumulation, neuronal loss and pronounced behavioral and cognitive deficits [13]. The mice were euthanized by carbon dioxide inhalation at room temperature, and the brains were rapidly removed and dissected on dry ice to obtain the cortex and hippocampus regions. The tissue samples were then frozen in liquid nitrogen and stored at -80 °C until analysis. The entire tissue harvesting and preparation process took 5–10 min to complete. Blood samples were collected following a previous study's protocol [14]. Briefly, we euthanized the mice with CO_2, exposed the heart, and collected blood with a one microliter syringe into an ethylenediaminetetraacetic acid (EDTA) tube. Brain tissue samples were then collected and transferred to designated collection tubes, which were properly labeled and stored at -80 °C until analysis.

HRMAS NMR

The ex vivo HRMAS proton (^{1}H) NMR measurements were performed at 4 °C on a Bruker AVANCE III HD 600 MHz 14.1 T spectrometer (Bruker BioSpin, Billerica, MA, USA), fitted with a ^{1}H-^{13}C-^{2}H (lock) HRMAS probe. Before measurements, frozen brain tissue samples were weighed (~10 mg) and blood samples were measured (10 µL) and loaded separately into a 4 mm HRMAS NMR rotor. For field locking, as well as to function as a reference for NMR measurements, 2.5 µL of D_2O was added into the rotor. Samples were measured at a spinning rate of 3600 Hz, using a rotor-synchronized Carr-Purcell-Meiboom-Gill (CPMG) method. When applicable, water was suppressed with presaturation. The spectral acquisition parameters were as follows: 5 s recycle time, 100 CPMG π pulses with a total mixing time of 55.6 ms, 16 K data points with a total acquisition time of 0.85 s, a spectral offset [O1P] of 4.7 ppm, and a spectral width of 16 ppm.

Data analyses

The HRMAS NMR spectra were analyzed using Bruker Topspin 3.6.2 software. Analyses included the following steps: 0.5 Hz line-broadening (exponential mode), one-time zero-fill to 32 K data points, Fourier transformation, automatic and manual phasing, baseline correction, and chemical shift calibration based on the lactate doublets at 1.32 ppm. Resonance peak curve-fitting was carried out with the deconvolution function in the software. Within the analyzed spectral region of 9.5 to 0.5 ppm (eliminating a water resonance region of 5.5–4.5 ppm), the total spectral intensity was used to normalize the measured and deconvoluted spectral peak intensities, to compare relative intensities across samples. The normalized peak intensities were then utilized to identify common spectral regions among the analyzed samples. A total of 51 spectral regions-of interest (ROI) were identified, including 40 regions common for all three tissue types, seven regions specifically for brain tissue, and four regions specifically for blood. These identified ROIs together with their potential contributing metabolites are listed in Supplementary Table S1, based on our systematic integrations of biological NMR data collected in the Human Metabolome Database (HMDB).

Due to limited sample sizes, two-sided, non-parametric Wilcoxon tests were carried out for univariable comparisons followed by false discovery rate (FDR) corrections. Hierarchical clustering analyses were conducted for each tissue type. Unsupervised multivariate principal component analysis (PCA) was calculated for all 51 identified spectral regions. All statistical analyses were performed using JMP Pro 16 (SAS Institute, Cary, NC, USA).

RESULTS

HRMAS NMR spectral regions of interest

HRMAS can produce high-resolution NMR spectra for intact brain tissues and blood plasma samples, in milligram (10 mg) and microliter (10 µl) scales, respectively. Spectra obtained from AD and WT brain cortex, hippocampus, and plasma are shown in Fig. 1A, respectively, with the averaged spectrum for each group together with standard deviations shown as shaded areas, while Fig. 1B presents unsupervised hierarchical clusters of their respective spectral regions, for these three sample types, respectively.

Spectral region differentiations between AD and WT groups

The apparent group differentiations presented in the heat maps can further be evaluated by univariate analyses of all ROIs measured from AD (female, $n = 8$; or female + male, $n = 15$) and WT ($n = 8$) subjects, as shown in Fig. 2 with the volcano plots for cortex, hippocampus and plasma, respectively.

Metabolomic differentiations between tested groups through principal component analysis

We then conducted unsupervised principal component analysis (PCA) on 51 spectral regions with cortex, hippocampus, and plasma together for samples from female AD and WT and tested the resulting principal components (PCs) for their utilities in

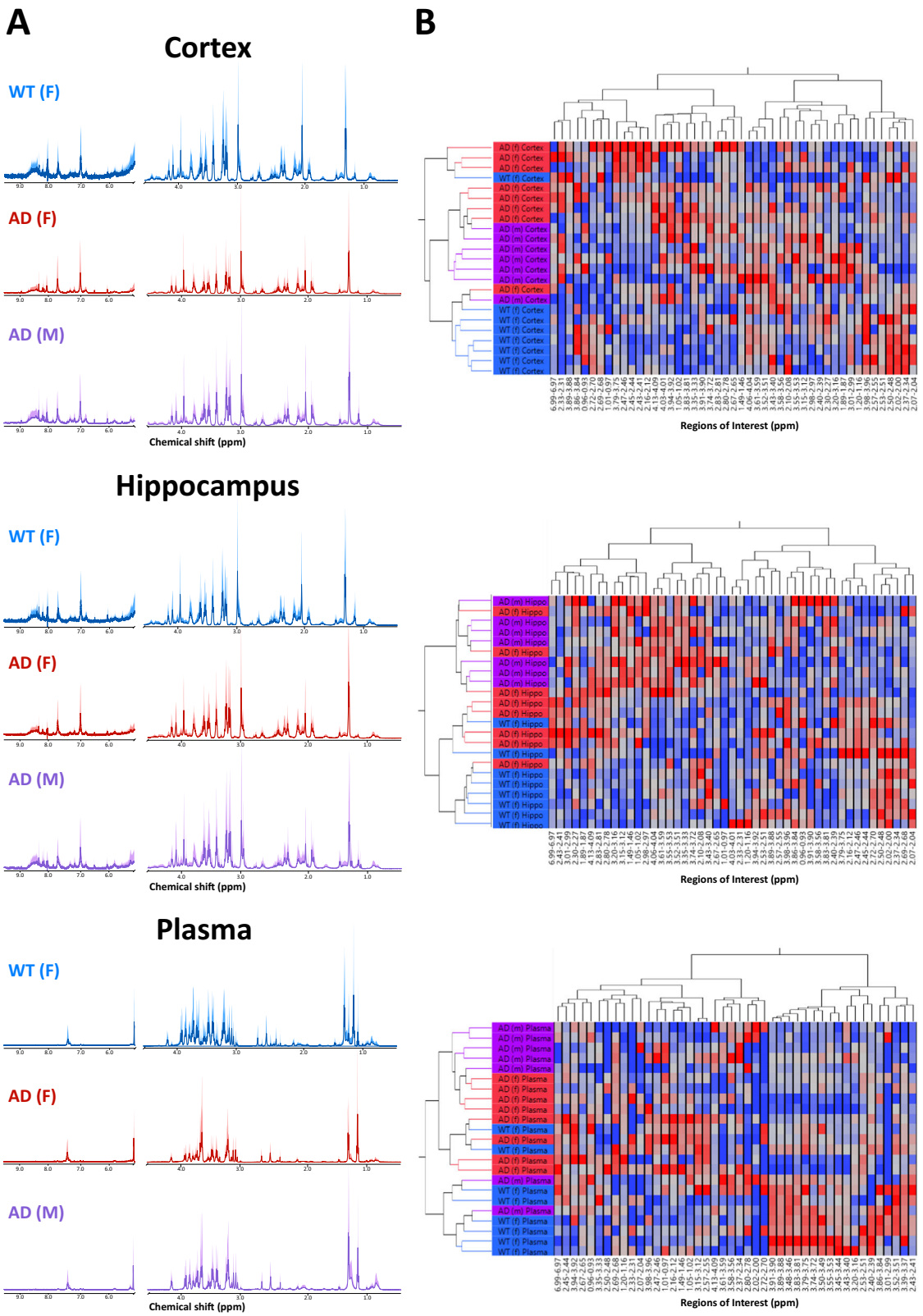

Fig. 1 Averaged HRMAS NMR spectra and hierarchical clusters. A Averaged HRMAS NMR spectra with standard deviations presented as shaded areas for cortex, hippocampus, and plasma, with WT female ($n = 8$), AD female ($n = 8$) and AD male ($n = 7$) groups presented separately for each tissue type. **B** Unsupervised hierarchical clusters of ROIs (x-axis) are plotted against the three mice groups. High spectral intensity in the ROIs are represented by red boxes, while low, in blue. Heat maps show clear distinctions between AD and WT for all three sample types. Using the top 15 rows as a threshold, the sensitivities [93.3, 93.3, 86.6] and specificities [87.5, 87.5, 75.0] are calculated for cortex, hippocampus, and plasma, respectively.

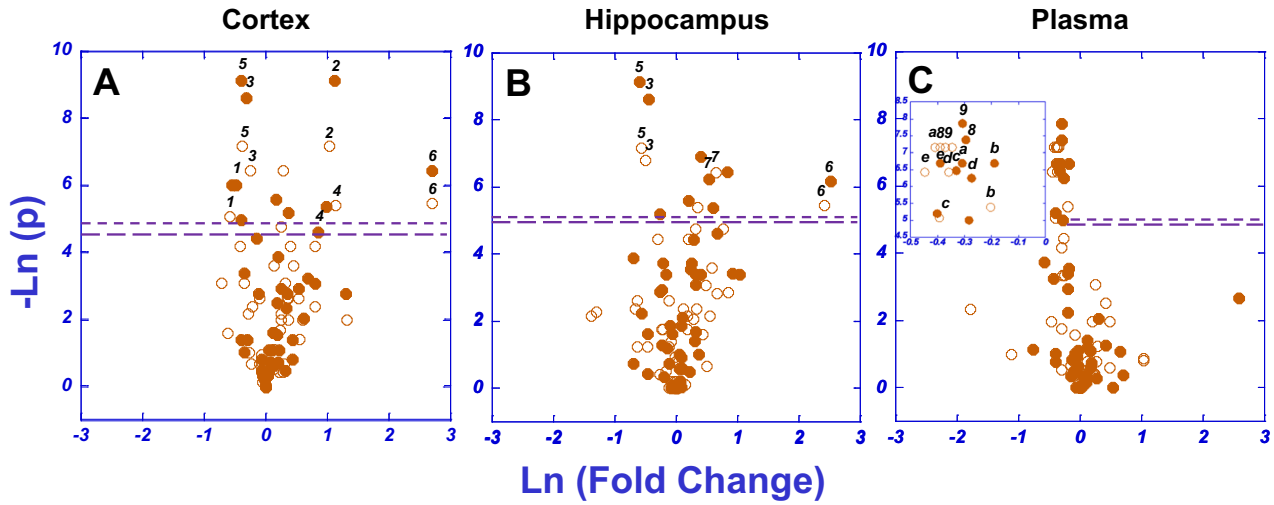

Fig. 2 Spectral regions differentiating AD and WT groups. Volcano plots of ln(Fold Change) vs. -ln(p), where Fold Change is the ratio of the AD mean over the control (i.e. WT) mean, and *p* values are calculated from Wilcoxon tests, for **A**. Cortex, **B**. Hippocampus, and **C**. Plasma, respectively. Solid circles represent results from all AD mice, including female and male, and open circles represent only female mice. Long dashed lines represent FDR significant levels for all AD animals, and short dashed lines represent FDR significant levels for only female animals. Fourteen spectral regions that were FDR significant based on Wilcoxon tests for all AD (solid circles) and female only (open circles) mice are labeled from 1–9 and a-e, representing various spectral ROIs in ppm: **1** 3.98–3.96; **2** 3.35–3.33; **3** 2.50–2.48; **4** 2.43–2.41; **5** 2.02–2.00; **6** 1.05–1.02; **7** 3.20–3.16; **8** 3.91–3.90; **9** 3.89–3.88; **a** 3.83–3.81; **b** 3.79–3.75; **c** 3.50–3.49; **d** 3.48–3.46; **e** 3.45-3.44.

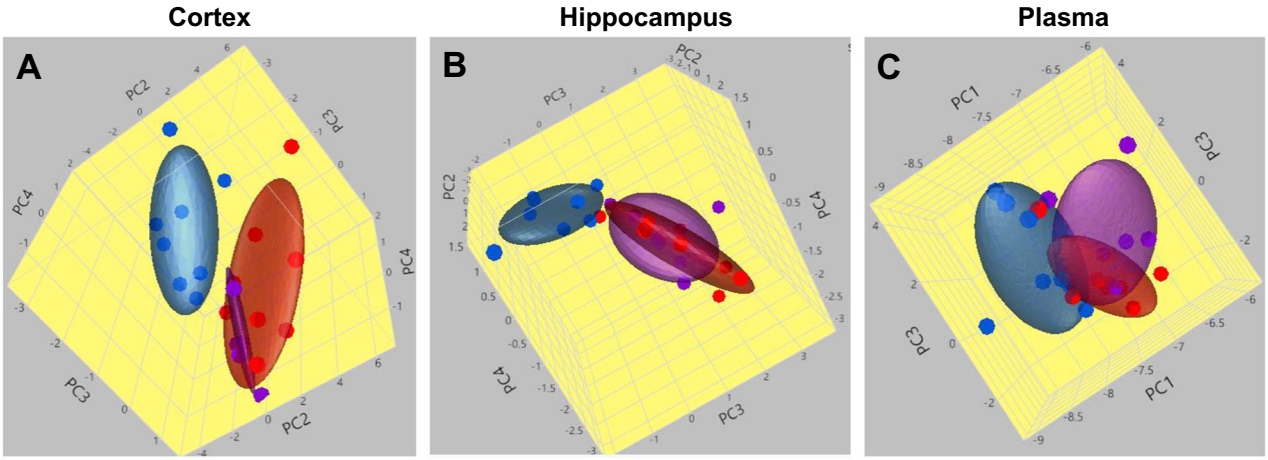

Fig. 3 Metabolomic ellipsoids differentiating AD from WT groups. 3D ellipsoids generated by the three most significant PCs as metabolomic profiles differentiating AD from WT animals as measured for **A**. Cortex, **B**. Hippocampus, and **C**. Plasma. Blue: WT, red: female AD, and purple: male AD.

differentiating between AD and WT groups, visualized in Fig. 3 as metabolomic ellipsoids. Male AD samples were not included in the PCA calculations to determine PCs. However, PCs determined from female AD samples were extrapolated to the males to visualize the density ellipsoids as seen in Fig. 3 as well as violin plots in Fig. 4. This enables the visual separation of WT and AD models using the most significant PCs, as such, the female ellipsoid (red) and male ellipsoid (purple) overlap across all sample types but differ from the WT ellipsoid (blue). Detailed results for the first five PCs for all three tissue types and for all animals (female AD and WT, as well as male AD) are presented in Fig. 4.

Significant spectral regions revealed by univariate wilcoxon and PCA tests

Figure 5 summarizes potential capabilities and contributions of individual spectral ROIs in differentiating WT from AD, either through their Wilcoxon tests, or according to their weighting, or loading factors (LF), towards the calculated PCs. PCA loading factors determine the weight for each spectral ROI's contribution towards the final value of the PC. Significant values are presented according to their measured trends, with red indicating AD means are higher than those of WT, while blue represents the opposite. The top 10 and 25% of ROIs that mostly contribute towards AD or WT are presented as orange or green, respectively.

Potential contributing metabolites

Univariable analyses of individual spectral regions and unsupervised multi-variable PCA produced results indicating potentials for their capabilities in differentiating AD from WT groups. Based on the summarized results shown in Fig. 5, and the potential contributing metabolites for each spectral ROI listed in Supplementary Table S1, Table 1 presents possible increased and decreased metabolite levels when comparing AD with WT. Metabolites listed in Table 1 met the following inclusion criteria: (1) having greater than or equal to 50% of their resonance peaks in the determined spectral regions, and (2) all the participating

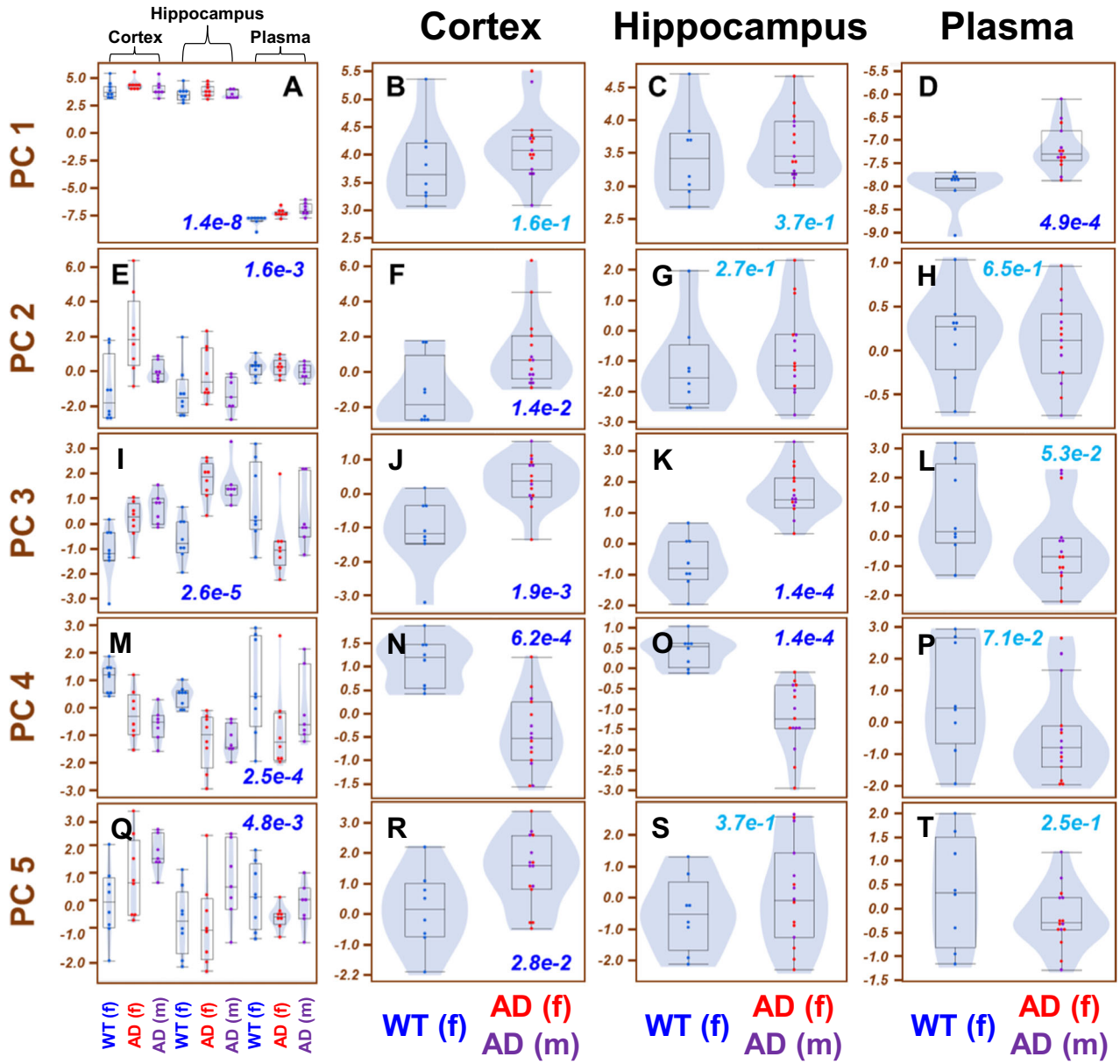

Fig. 4 Principal components for WT and AD. The five PCs present varied potentials of differentiating WT from AD for three tested tissue types. PC1 results are shown in **A**–**D**, PC2 in **E**–**H**, PC3 in **I**–**L**, PC4 in **M**–**P**, and PC5 in **Q**–**T**. A summary of all violin plots for each PC is shown in the first column **A**, **E**, **I**, **M**, **Q**, and results for each tissue type are presented in the other columns, namely, cortex **B**, **F**, **J**, **N**, **R**, hippocampus **C**, **G**, **K**, **O**, **S**, and plasma **D**, **H**, **L**, **P**, **T**. Statistically significant *p*-values ($p < 0.05$) calculated from Wilcoxon tests are presented in dark blue, and not significant *p*-values are in light blue. The most significant PCs are PC3 and PC4 for both cortex and hippocampus, and PC1 for plasma. Error bars represent standard deviation.

spectral regions for a specific metabolite following the same increasing or decreasing trend, i.e., no conflicting trend existed among the spectral regions of a potential contributing metabolite. A potential metabolite in Table 1 is listed in one of these three categories: (1) a metabolite presented in **Bold** has more than 50% of its potential contributing spectral regions as significantly different between compared groups, and at least one of these spectral regions demonstrates significant differences after FDR corrections; (2) presented in ***Italic Bold***, are metabolites that have more than 50% of their potential contributing ROIs as significantly different between case and control groups, but none of them are significant after FDR corrections; and (3) other remaining potential metabolites that met the inclusion criteria stated above, but fail to meet the significance criteria described appear as regular text. Our method of metabolite identification relies on the regions of interest, which are based upon chemical shift values observed in spectra and reported by HMDB. As a result, while any derived metabolites of interest *may* exist in our spectra, its existence is not absolute. Additional methods can be utilized to confirm our findings, such as multidimensional NMR, other analytical methods such as mass spectrometry, and references to additional NMR databases.

DISCUSSION

Our results provide support for widespread altered metabolomics in AD conditions, associating metabolomic shifts across brain tissue and blood plasma.

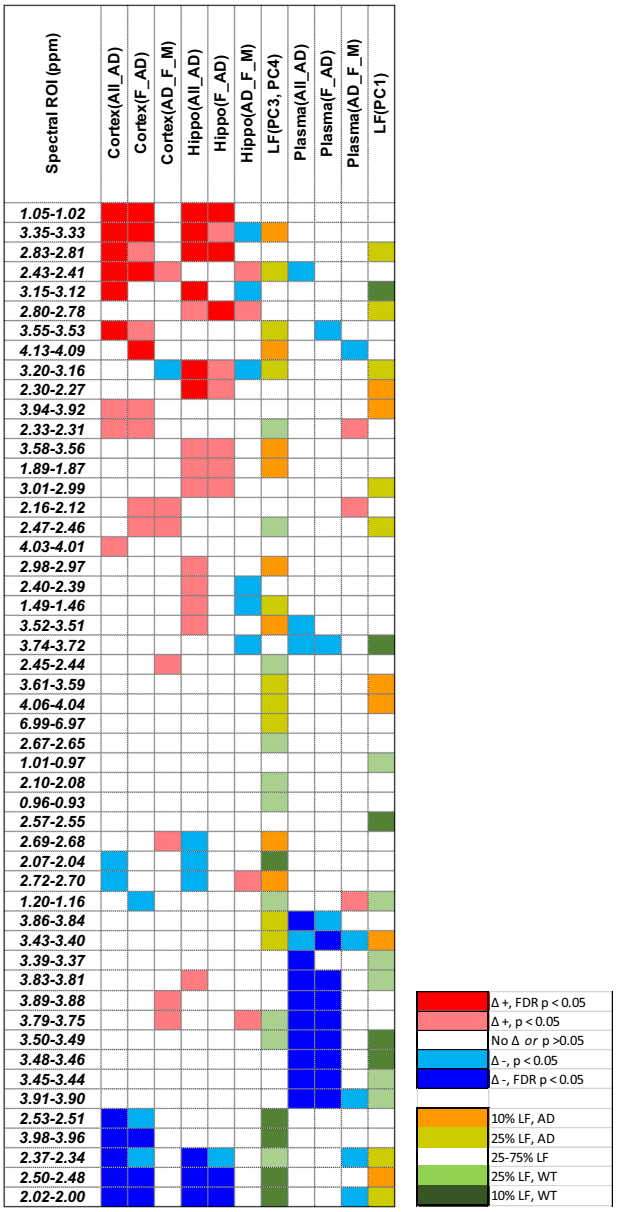

Fig. 5 Spectral ROI differentiations of WT and AD and their contributions to differentiating PCs. Δ represents the difference of AD – WT. LF stands for PCA loading factor for a particular spectral ROI.

Alterations in glucose metabolism

Under healthy conditions, glucose is the sole source of energy for the brain. Abnormalities in its metabolism are key indicators of declining brain health, contributing to neuroinflammation, neurofibrillary plaques and tangles, oxidative stress, and malfunctions in other related systems [15].

Normally, lactic acid is produced during glycolysis via pyruvate reduction; however, abnormal mitochondrial function and/or lactic acid clearance can disrupt lactic acid homeostasis, thereby affecting physiological brain functions [16–19]. Numerous studies report a prominent role for lactate in regulating brain function, providing energy fuel for neurons, and cellular signaling [18–22]. However, alterations in lactate homeostasis can result in neurological dysfunction and further the development of neuropsychiatric disorders [19–21,23]. We detected significantly increased levels of lactic acid in both cortex and hippocampus and non-significant increases in blood plasma, consistent with prior findings [19, 24]. Increased lactate secretion by astrocytes was shown to be present in neurodegenerative diseases, favoring Aβ plaque deposition, while increased lactate uptake by neurons may cause reduced mitochondrial activity, cytoplasmic acidification, and neuronal death [19, 25]. Furthermore, reduced activity of mitochondrial pyruvate carriers has been reported in neurodegenerative states, leading to excess cytoplasmic pyruvate and aberrant anaerobic glycolysis, thus aggravating lactate accumulation and neuroinflammation [26]. We observed increases in pyruvic acid across all tissues and biofluids, corroborating these results.

Glucose-6-phosphate was decreased in plasma, but no significant differences were observed in brain tissue. This suggests its conversion to pyruvate via glycolysis but may also indicate downregulation of the pentose phosphate pathway, which generates metabolites that alleviate redox stress for neuronal protection [27, 28].

Levels of trans-aconitic acid, a Krebs cycle metabolite, were increased in cortex and hippocampal tissue but decreased in blood plasma. Similarly, cis-aconitic acid, an intermediate metabolite in the isomerization from citrate to isocitrate, was seen to decrease in plasma, which aligns with our observed increase in citrate levels in plasma. In a previous study of Parkinson's disease, decreases in cis-aconitic acid were noted in patient blood samples, alluding to its role in neurodegeneration through downregulation of Krebs Cycle [27]. As a competitive inhibitor for aconitase (a Krebs Cycle enzyme), increased trans-aconitic acid in brain tissue may suggest further inhibition of the Krebs Cycle at these sites. On the other hand, decreased citrate levels in the hippocampus may indicate its conversion to pyruvic acid (increasing across all samples) and reduced anti-inflammatory activity in the brain [29].

Oxidative stress leading to brain dysfunction

Abnormal energy metabolism, particularly via mitochondrial dysfunction, has long been associated with AD pathophysiology through oxidative stress in neurodegeneration and tau hyperphosphorylation [30, 31]. For instance, galactitol, a reduced product of galactose, has been documented to accumulate in neurons and generate free radicals by impacting the electron transport chain, resulting in oxidative stress and mitochondrial dysfunction [32–35]. Here, a decrease in galactitol in the cortex (significant) and hippocampus (non-significant) was observed. Decreased levels of galactitol may result from its oxidation into aldehyde and hydrogen peroxide [36], further exacerbating oxidative stress in cells. Interestingly, Tsakiris et al. found that supplementation of sulfhydryl-containing antioxidants, such as L-cysteine and glutathione, reverses the oxidative stress impact of galactitol by binding to free radicals [34]. Our findings of significant decreases in cortex L-cysteine are corroborated by previous studies noting its 3-fold decrease in AD versus healthy rodent brains [33].

Moreover, we found an increase in propionate (which has been associated with an increased risk of cognitive decline in human subjects [37]) in both brain tissue and blood plasma, complementing results from prior studies using saliva samples [38]. MMA and propionic acidemia, characterized by increased concentrations of free MMA and propionate, can hinder mitochondrial function by disrupting Krebs Cycle and electron transport chain, producing reactive oxygen species (ROS) that lead to neurodegeneration and AD-related pathophysiology [39–41].

Finally, we observed significantly decreased betaine (trimethylglycine) levels in plasma. Betaine was demonstrated to have a positive impact in alleviating neurodegenerative cognitive deficits, attenuating tau phosphorylation, and decreasing Aβ accumulation [42]. By donating methyl groups, betaine can convert homocysteine to methionine, a potential antioxidant [43]. Decreased

Table 1. Potential metabolites associated with AD vs. WT presented in spectral regions.

Location	Decrease				Increase			
Cortex	**Galactit#**	**iPrOH**	**L-Cys#**		**GlycA**	**L-Lac#**		
	3-HIVA	***DMA***	***EtOH***	***iBuA***	***3-HMGA***	***Biopterin***	***Creat#***	***Gly#***
	UPA				***GlycolA***	***Hypot***	***MeOH***	***OxoadipA***
					PropA	***PyrA#***	***Theo***	
	1,3-DMU	2-AIBA	2-H2MBA	2-H3MBA	2-KBA	3-ClTyr	7-MX	9-MU
	3-AIBA	3-MX	Caff	Creatin#	Aten	Bet#	Biotin	D-Fru
	Glycogen	Ribo	Sar#	SyrA	D-GlcA	D-Xylit	DL-2-AOA	EA
	Tau	ThreoA			Famot	GAA	GlucA	GlucL
					Gly-Gly	Glycer	HPAG	L-Arg#
					L-Cyst#	L-NorLeu	L-α-ABA#	Lactul
					MMA#	Neo	NMN	O-PEA
					Ribitol#	rT	SDMA	ShikA
					SuccA#	T	THF	trans-AA
					Ψ			
Hippo	***3-HIVA***	***DMA***	***UPA***		***2-KBA***	***9-MU***	***GABA#***	***MeOH***
					MMA#	***PropA***	***T***	***α-KIVA***
	2-H3MBA	7-MX	AcGly	Cit#	1,3-DMU	1-BuOH	2,3-BD	2-AIBA
	Creat#	EtOH	GAA	Galactit#	3-ClTyr	3-MX	4-MeOPAA	Bet#
	Gly#	GlycolA	Malic acid#	O-PEA	Biotin	Caff	Creatin#	D-Threitol
	SyrA				D-Xylit	DL-2-AOA	EA	GBP
					Gly-Gly	HPAG	L-Lac#	L-NorLeu
					NMN	PPGly	PyrA#	Sar#
					SuccA#	Tau	trans-AA	
Plasma	**1,3-DMU**	**3,7-DMU**	**AcAc**	**cis-AA#**				
	D-Glc#	**DHU**	**G6P#**	**Maltotet**				
	MIAA	**PropGly**	**Suc**	**Tau**				
	β-GlcNAc							
	7-MX	***Bet#***	***D-Xylit***	***GAA***				
	Gly#	***Gly-Gly***	***HPA***	***L-Idit***				
	Mannitol#	***MANNOHEP***	***Ribitol#***	***SyrA***				
	trans-AA							
	1,5-AS#	2-KBA	2-Pyr	3-DHDMBAP	1-BuOH	2-AIBA	Cadav	Cit#
	3-HIVA	3-MX	4-Hyp#	5,6,7,8-THF	Creat#	DL-O-PSer	DMA	EtOH
	9-MU	All	Aten	Caff	Galactit#	GlycolA	Hypot	iBuGly
	Chol#	D-Gal	D-GlcA	D-Malt	L-Lac#	MeOH	PropA	PSer
	D-t-ICA	D-Xyl	DHT	Glycogen	PyrA#	Sar#	StearA	
	HexCarn	HomovA	Isomaltose	L-Arab				
	L-Leu#	L-PipA	L-Pro#	NMN				
	PipA	Pseudoeph	SeCyst	Sphing				
	SuccA#	T4	THFA	UPA				
	Venlaf							

Increase or decrease refers to mean values of AD compared to WT. **Bold**: significant after FDR corrections, ***Italic Bold*** : significant only before FDR corrections (see text for details). Single underlined metabolites presented same trends in at least two tissue types of cortex, hippocampus and plasma, with at least one comparison showing one of the two categorized significance levels (in **Bold** or ***Italic Bold***). Double underlined metabolites presented opposite trends in different tissue types, with the same significance rule."#" represents metabolites relevant to AD. Abbreviations can be found in Supplementary Table S1.

betaine could explain AD pathological alterations; however, the observed increasing trends in brain tissues (non-significant) conflict with previously reported results [44, 45]. In our study, increased betaine may be in response to oxidative stress; however, further testing is required to verify this finding and elucidate its potential neuroprotective properties [46].

Interactions with other neural pathways

AD pathophysiology is highly complex, integrating diverse metabolic mechanisms, thereby impacting the neurochemistry of learning and memory. Taurine, a well-researched metabolite in AD, is known for its neuroprotective effects [47], ameliorating the behavioral deficiencies of AD [48]. However, proposed

mechanisms-of-action have thus far been inconsistent and contradictory. Though taurine has been reported to directly bind to oligomeric Aβ [46], others propose it effects glutamatergic or GABAergic transmission systems (with no impact on Aβ plaque concentrations/formations) to potentially decrease neuronal vulnerability to excitotoxic stress [48, 49]. We found significantly decreased levels of taurine in the cortex and plasma of AD mice, which is consistent with previous data in human AD patients [47]. This may also explain observed increases in hypotaurine, which can be converted to taurine by hypotaurine dehydrogenase, in the same regions, in response to oxidative stress [50]. Contrastingly, the observed upregulation of taurine (non-significant) in the hippocampus may be a response to AD pathological changes. Furthermore, increased GABA was also observed in the hippocampus, supporting the hypothesis that taurine activates GABA receptors. GABA dysregulation in AD studies have thus far provided contradictory results; while it was previously thought to contribute to neurodegeneration and cognitive decline, recently, research postulates that GABA may alleviate AD pathology, cognitive impairment, and regulate neurogenesis [51, 52].

Moreover, we observed decreased dimethylamine (DMA) in brain tissues. DMA is a breakdown product of asymmetric dimethylarginine (ADMA), an inhibitor of nitic oxide (NO) synthase, via dimethylarginine dimethylaminohydrolase (DDAH). Due to increasing oxidative stress during AD, DDAH activity is inhibited [53, 54], decreasing production of DMA. Interestingly, NO can play a dual role, acting as both a neurotoxin that exacerbates AD and as an unconventional neurotransmitter with protective functions, inducing learning, memory, and neuroplasticity. As such, regulating NO metabolism through DDAH activity may be a potential target for treating AD [55–57].

Correlating blood plasma and brain tissue metabolites

By observing the metabolic flux in tissue and blood plasma samples, our goal is to investigate the potential relationship between different sample types for AD detection and prognosis. Several previously discussed metabolites displayed the same trends across all sample types (lactic acid, pyruvic acid, and propionate), and were hypothesized to contribute to AD through glucose oxidation and/or mitochondrial dysfunction. Other metabolites, while not directly related to energy metabolism, also display the same trends across all tissues, namely, methanol and 3-hydroxyisovaleric acid (3-HIVA).

Increased levels of methanol were observed across all samples. Methanol is known to cause neuronal tau phosphorylation and contributes to the deposition of Aβ protein in the hippocampus [58]. Furthermore, its oxidation metabolites, formaldehyde and formic acid, have been shown to cause similar effects in vitro [59, 60]. On the other hand, 3-HIVA levels were decreased in all samples. Previous studies report contradictory results regarding the presence of 3-HIVA in AD [29, 61]. Decreased levels of 3-HIVA, a byproduct of leucine metabolism, may result from reduced leucine levels (plasma, not significant), correlating to severe cognitive decline [62].

However, further research is clearly needed to elucidate the patterns between tissue and blood metabolites, their inter-relations, distinctions, and underlying mechanisms. Potential avenues include multidimensional NMR to reduce spectral overlap typically observed in 1D spectroscopy. Future work can also incorporate complementary analytical techniques, such as mass spectrometry to improve the detection of metabolites in low concentrations. For example, previous studies utilizing liquid chromatography-mass spectrometry (LC-MS) have demonstrated metabolomic changes in early-stage AD brain tissue corresponding to altered glucose metabolism and impaired Kreb's cycle [63]. Moreover, other LC-MS metabolomics work have identified sex-specific metabolic serum and tissue changes in early and late-onset AD mice models, primarily changes in lipids, which can provide complementary information to this work [64]. We are also interested in investigating the blood and brain metabolomics of mice with other neurological deficits, such as mild cognitive impairment (MCI), to identify potential overlaps between MCI and AD conditions.

In this investigation we also identified two metabolites, syringic acid and 7-methylxanthine, commonly found in food and plants. Their presence warrants further investigation into the diet and handling of the mice, while exploring potential interactions between diet and neuropathy. Moreover, a greater sample size can increase the statistical strength of our findings. Furthermore, this current study only used female wild-type models as the control since AD has been reported to be more prevalent in women and female animal models, with women having a higher risk of developing AD, where disease progression and severity differ from men [65–67]. By focusing on female WT mice, this work aimed to better mimic the female-dominant prevalence observed in human AD cases and to explore potential sex-specific responses to future treatment interventions and factors contributing to AD development (i.e., anesthesia/surgery) in our model [68]. However, this is a limitation of our current study, not accounting for the full spectrum of sex-related differences in AD pathology. This will be addressed in future work where we will include both male and female mice, as well as a range of ages, in the WT condition to capture a more comprehensive view of AD pathophysiological changes ultimately leading to more robust and generalizable findings.

In conclusion, we demonstrate that HRMAS NMR can be used to differentiate between AD and WT from blood plasma and brain tissue in AD mouse models, where measured metabolic profiles vary for cortex, hippocampus, and plasma. We report significant alterations in metabolites associated with glucose and energy metabolism, oxidative stress and those interacting with neural pathways. These findings have potential to be implemented into in vivo mice evaluations, leading to new, non-invasive diagnostic methods for AD. The potential of this work can enable clinicians to monitor the effects of prospective future therapies and progress our current understanding of AD metabolic mechanisms.

DATA AVAILABILITY

Data is available to readers upon request.

REFERENCES

1. 2023 Alzheimer's disease facts and figures. Alzheimers Dement. 2023;19:1598-695. https://doi.org/10.1002/alz.13016.
2. Scheltens P, De Strooper B, Kivipelto M, Holstege H, Chételat G, Teunissen CE, et al. Alzheimer's disease. Lancet. 2021;397:1577–90. https://doi.org/10.1016/s0140-6736(20)32205-4
3. Livingston G, Sommerlad A, Ortega V, Costafreda SG, Huntley J, Ames D, et al. Dementia prevention, intervention, and care. Lancet. 2017;390:2673–734. https://doi.org/10.1016/s0140-6736(17)31363-6
4. Ardanaz CG, Ramírez MJ, Solas M. Brain metabolic alterations in Alzheimer's disease. Int J Mol Sci. 2022;23:3785. https://doi.org/10.3390/ijms23073785
5. Yin F, Sancheti H, Patil I, Cadenas E. Energy metabolism and inflammation in brain aging and Alzheimer's disease. Free Radic Biol Med. 2016;100:108–22. https://doi.org/10.1016/j.freeradbiomed.2016.04.200
6. Braak H, Alafuzoff I, Arzberger T, Kretzschmar H, Del Tredici K. Staging of Alzheimer disease-associated neurofibrillary pathology using paraffin sections and immunocytochemistry. Acta Neuropathol. 2006;112:389–404. https://doi.org/10.1007/s00401-006-0127-z
7. Braak H, Braak E. Frequency of stages of Alzheimer-related lesions in different age categories. Neurobiol Aging. 1997;18:351–7. https://doi.org/10.1016/S0197-4580(97)00056-0
8. Dienel GA. Metabolomic assays of postmortem brain extracts: pitfalls in extrapolation of concentrations of glucose and amino acids to metabolic dysregulation in vivo in neurological diseases. Neurochem Res. 2019;44:2239–60. https://doi.org/10.1007/s11064-018-2611-y
9. Drummond E, Wisniewski T. Alzheimer's disease: experimental models and reality. Acta Neuropathol. 2017;133:155–75. https://doi.org/10.1007/s00401-016-1662-x
10. Angioni D, Delrieu J, Hansson O, Fillit H, Aisen P, Cummings J, et al. Blood biomarkers from research use to clinical practice: what must be done? a report

from the EU/US CTAD Task Force. J Prev Alzheimers Dis. 2022;9:569–79. https://doi.org/10.14283/jpad.2022.85
11. Füzesi MV, Muti IH, Berker Y, Li W, Sun J, Habbel P, et al. High resolution magic angle spinning proton NMR Study of Alzheimer's Disease with mouse models. Metabolites. 2022;12:253. https://doi.org/10.3390/metabo12030253
12. Cheng LL. High resolution magic angle spinning NMR for intact biological specimens analyses: initial discovery, recent developments, and future directions. NMR Biomed. 2023;36:e4684. https://doi.org/10.1002/nbm.4684
13. Oblak AL, Lin PB, Kotredes KP, Pandey RS, Garceau D, Williams HM, et al. Comprehensive evaluation of the 5XFAD mouse model for preclinical testing applications: A MODEL-AD Study. Front Aging Neurosci. 2021;13:713726.
14. Lu J, Liang F, Bai P, Liu C, Xu M, Sun Z, et al. Blood tau-PT217 contributes to the anesthesia/surgery-induced delirium-like behavior in aged mice. Alzheimers Dement. 2023;19:4110–26. https://doi.org/10.1002/alz.13118
15. Sacks D, Baxter B, Campbell BCV, Carpenter JS, Cognard C, Dippel D, et al. Multisociety consensus quality improvement revised consensus statement for endovascular therapy of acute ischemic stroke. Int J Stroke. 2018;13:612–32. https://doi.org/10.1177/1747493018778713
16. Levy B. Lactate and shock state: the metabolic view. Curr Opin Crit Care. 2006;12:315–21. https://doi.org/10.1097/01.ccx.0000235208.77450.15
17. Proia P, Di Liegro CM, Schiera G, Fricano A, Di Liegro I. Lactate as a metabolite and a regulator in the central nervous system. Int J Mol Sci. 2016;17:1450. https://doi.org/10.3390/ijms17091450
18. Salmina AB, Kuvacheva NV, Morgun AV, Komleva YK, Pozhilenkova EA, Lopatina OL, et al. Glycolysis-mediated control of blood-brain barrier development and function. Int J Biochem Cell Biol. 2015;64:174–84. https://doi.org/10.1016/j.biocel.2015.04.005
19. Chen X, Zhang Y, Wang H, Liu L, Li W, Xie P. The regulatory effects of lactic acid on neuropsychiatric disorders. Discov Ment Health. 2022;2:8. https://doi.org/10.1007/s44192-022-00011-4
20. Wu A, Lee D, Xiong WC. Lactate metabolism, signaling, and function in brain development, synaptic plasticity, angiogenesis, and neurodegenerative diseases. Int J Mol Sci. 2023;24:13398. https://doi.org/10.3390/ijms241713398
21. Li R, Yang Y, Wang H, Zhang T, Duan F, Wu K, et al. Lactate and lactylation in the brain: current progress and perspectives. Cell Mol Neurobiol. 2023;43:2541–55. https://doi.org/10.1007/s10571-023-01335-7
22. Magistretti PJ, Allaman I. Lactate in the brain: from metabolic end-product to signalling molecule. Nat Rev Neurosci. 2018;19:235–49. https://doi.org/10.1038/nrn.2018.19
23. Pan L, Feng F, Wu J, Fan S, Han J, Wang S, et al. Demethylzeylasteral targets lactate by inhibiting histone lactylation to suppress the tumorigenicity of liver cancer stem cells. Pharmacol Res. 2022;181:106270. https://doi.org/10.1016/j.phrs.2022.106270
24. Harris RA, Tindale L, Lone A, Singh O, Macauley SL, Stanley M, et al. Aerobic glycolysis in the frontal cortex correlates with memory performance in wild-type mice but not the APP/PS1 mouse model of cerebral amyloidosis. J Neurosci. 2016;36:1871–8. https://doi.org/10.1523/jneurosci.3131-15.2016
25. Schwartz L, Peres S, Jolicoeur M, da Veiga Moreira J. Cancer and Alzheimer's disease: intracellular pH scales the metabolic disorders. Biogerontology. 2020;21:683–94. https://doi.org/10.1007/s10522-020-09888-6
26. Garabadu D, Agrawal N, Sharma A, Sharma S. Mitochondrial metabolism: a common link between neuroinflammation and neurodegeneration. Behav Pharmacol. 2019;30:642–52. https://doi.org/10.1097/fbp.0000000000000505
27. Gonzalez-Riano C, Saiz J, Barbas C, Bergareche A, Huerta JM, Ardanaz E, et al. Prognostic biomarkers of Parkinson's disease in the Spanish EPIC cohort: a multiplatform metabolomics approach. NPJ Parkinsons Dis. 2021;7:73. https://doi.org/10.1038/s41531-021-00216-4
28. Tang BL. Neuroprotection by glucose-6-phosphate dehydrogenase and the pentose phosphate pathway. J Cell Biochem. 2019;120:14285–95. https://doi.org/10.1002/jcb.29004
29. de Leeuw FA, Peeters CFW, Kester MI, Harms AC, Struys EA, Hankemeier T, et al. Blood-based metabolic signatures in Alzheimer's disease. Alzheimers Dement. 2017;8:196–207. https://doi.org/10.1016/j.dadm.2017.07.006
30. Bhatia V, Sharma S. Role of mitochondrial dysfunction, oxidative stress and autophagy in progression of Alzheimer's disease. J Neurol Sci. 2021;421:117253. https://doi.org/10.1016/j.jns.2020.117253
31. Misrani A, Tabassum S, Yang L. Mitochondrial dysfunction and oxidative stress in Alzheimer's disease. Front Aging Neurosci. 2021;13:617588. https://doi.org/10.3389/fnagi.2021.617588
32. Shwe T, Pratchayasakul W, Chattipakorn N, Chattipakorn SC. Role of D-galactose-induced brain aging and its potential used for therapeutic interventions. Exp Gerontol. 2018;101:13–36. https://doi.org/10.1016/j.exger.2017.10.029
33. Luo Y, Zhang L, Liu W, Yu Y, Tian Y. A single biosensor for evaluating the levels of copper ion and L-Cysteine in a live rat brain with Alzheimer's disease. Angew Chem Int Ed Engl. 2015;54:14053–6. https://doi.org/10.1002/anie.201508635
34. Nam SM, Hwang H, Seo M, Chang B, Kim H, Choi S, et al. Gintonin attenuates D-Galactose-Induced hippocampal senescence by improving long-term hippocampal potentiation, neurogenesis, and cognitive functions. Gerontology. 2018;64:562–75. https://doi.org/10.1159/000491113
35. Tsakiris S, Schulpis KH, Marinou K, Behrakis P. Protective effect of L-cysteine and glutathione on the modulated suckling rat brain Na+, K+, -ATPase and Mg2+ -ATPase activities induced by the in vitro galactosaemia. Pharmacol Res. 2004;49:475–9. https://doi.org/10.1016/j.phrs.2003.11.006
36. Lekchand Dasriya V, Samtiya M, Dhewa T, Puniya M, Kumar S, Ranveer S, et al. Etiology and management of Alzheimer's disease: potential role of gut microbiota modulation with probiotics supplementation. J Food Biochem. 2022;46:e14043. https://doi.org/10.1111/jfbc.14043
37. Neuffer J, Gonazalez-Dominguez R, Lefvre-Arbogast S, Low DT, Driollet B, Helmer C, et al. Exploration of the gut-brain axis through metabolomics identifies serum propionic acid associated with higher cognitive decline in older persons. Nutrients. 2022;14:4688. https://doi.org/10.3390/nu14214688
38. Figueira J, Jonsson P, Nordin Adolfsson A, Adolfsson R, Nyberg L, Öhman A. NMR analysis of the human saliva metabolome distinguishes dementia patients from matched controls. Mol Biosyst. 2016;12:2562–71. https://doi.org/10.1039/c6mb00233a
39. Jodeiri Farshbaf M, Kiani-Esfahani A. Succinate dehydrogenase: prospect for neurodegenerative diseases. Mitochondrion. 2018;42:77–83. https://doi.org/10.1016/j.mito.2017.12.002
40. Fontella FU, Pulronik V, Gassen E, Wannmacher CM, Klein AB, Wajner M, Dutra-Filho CS. Propionic and L-methylmalonic acids induce oxidative stress in brain of young rats. Neuroreport. 2000;11:541–4. https://doi.org/10.1097/00001756-200002280-00023
41. Wang C, Zhang Y, Shu J, Gu C, Yu Y, Liu W. Association between methylmalonic acid and cognition: a systematic review and meta-analysis. Front Pediatr. 2022;10:901956. https://doi.org/10.3389/fped.2022.901956
42. Bhatt M, Di Iacovo A, Romanazzi T, Roseti C, Bossi E. Betaine-the dark knight of the brain. Basic Clin Pharmacol Toxicol. 2023;133:485–95. https://doi.org/10.1111/bcpt.13839
43. Zhao G, He F, Wu C, Li P, Li N, Deng J, et al. Betaine in inflammation: mechanistic aspects and applications. Front Immunol. 2018;9:1070. https://doi.org/10.3389/fimmu.2018.01070
44. Ibi D, Kondo S, Ohmi A, Kojima Y, Nakasai G, Takaba R, et al. Preventive effect of betaine against cognitive impairments in amyloid β peptide-injected mice through Sirtuin1 in hippocampus. Neurochem Res. 2022;47:2333–44. https://doi.org/10.1007/s11064-022-03622-z
45. Puris E, Kouril S, Najdekr K, Auriola S, Loppi S, Korhonen P, et al. Metabolomic, lipidomic and proteomic characterisation of lipopolysaccharide-induced inflammation mouse model. Neuroscience. 2022;496:165–78. https://doi.org/10.1016/j.neuroscience.2022.05.030
46. Jang H, Lee S, Choi SL, Kim HY, Baek S, Kim Y. Taurine directly binds to oligomeric amyloid-β and recovers cognitive deficits in Alzheimer model mice. Adv Exp Med Biol. 2017;975:233–41. https://doi.org/10.1007/978-94-024-1079-2_21
47. Menzie J, Pan C, Prentice H, Wu JY. Taurine and central nervous system disorders. Amino Acids. 2014;46:31–46. https://doi.org/10.1007/s00726-012-1382-z
48. Louzada PR, Paula Lima AC, Mendonca-Silva DL, Noël F, De Mello FG, Ferreira ST. Taurine prevents the neurotoxicity of beta-amyloid and glutamate receptor agonists: activation of GABA receptors and possible implications for Alzheimer's disease and other neurological disorders. FASEB J. 2004;18:511–8. https://doi.org/10.1096/fj.03-0739com
49. Oh SJ, Lee HJ, Jeong YJ, Nam KR, Kang KJ, Han SJ, et al. Evaluation of the neuroprotective effect of taurine in Alzheimer's disease using functional molecular imaging. Sci Rep. 2020;10:15551. https://doi.org/10.1038/s41598-020-72755-4
50. Huang Y, Liu Z, Liu S, Song F, Hu X, Qin Y, et al. Urine metabolic profiling of dementia rats with vital energy deficiency using ultra-high-performance liquid chromatography coupled with an orbitrap mass spectrometer. J Sep Sci. 2022;45:507–17. https://doi.org/10.1002/jssc.202100837
51. Sibbe M, Kulik A. GABAergic regulation of adult hippocampal neurogenesis. Mol Neurobiol. 2017;54:5497–510. https://doi.org/10.1007/s12035-016-0072-3
52. Carello-Collar G, Bellaver B, Ferreira PCL, Ferrari-Souza JP, Ramos VG, Therriault J, et al. The GABAergic system in Alzheimer's disease: a systematic review with meta-analysis. Mol Psychiatry. 2023;28:5025–36. https://doi.org/10.1038/s41380-023-02140-w
53. Chen S, Li N, Deb-Chatterji M, Dong Q, Kielstein JT, Weissenborn K, et al. Asymmetric dimethyarginine as marker and mediator in ischemic stroke. Int J Mol Sci. 2012;13:15983–6004. https://doi.org/10.3390/ijms131215983
54. Hulin JA, Gubareva EA, Jarzebska N, Rodionov RN, Mangoni AA, Tommasi S. Inhibition of dimethylarginine dimethylaminohydrolase (DDAH) enzymes as an emerging therapeutic strategy to target angiogenesis and vasculogenic mimicry in cancer. Front Oncol. 2019;9:1455. https://doi.org/10.3389/fonc.2019.01455
55. Paul V, Ekambaram P. Involvement of nitric oxide in learning & memory processes. Indian J Med Res. 2011;133:471–8.

56. Azargoonjahromi A. Dual role of nitric oxide in Alzheimer's disease. Nitric Oxide. 2023;134-135:23–37. https://doi.org/10.1016/j.niox.2023.03.003
57. Selley ML. Homocysteine increases the production of asymmetric dimethylarginine in cultured neurons. J Neurosci Res. 2004;77:90–3. https://doi.org/10.1002/jnr.20070
58. Yang M, Lu J, Miao J, Rizak J, Yang J, Zhai R, et al. Alzheimer's disease and methanol toxicity (part 1): chronic methanol feeding led to memory impairments and tau hyperphosphorylation in mice. J Alzheimers Dis. 2014;41:1117–29. https://doi.org/10.3233/jad-131529
59. He R, Lu J, Miao J. Formaldehyde stress. Sci China Life Sci. 2010;53:1399–404. https://doi.org/10.1007/s11427-010-4112-3
60. Tong Z, Luo W, Wang Y, Yang F, Han Y, Li H, et al. Tumor tissue-derived formaldehyde and acidic microenvironment synergistically induce bone cancer pain. PLoS ONE. 2010;5:e10234. https://doi.org/10.1371/journal.pone.0010234
61. Kim DH, Gim J-A, Yoon D, Kim S, Kim H-S. Metabolomics and mitochondrial dysfunction in Alzheimer's disease. Genes & Genomics. 2017;39:295–300. https://doi.org/10.1007/s13258-016-0494-3
62. Conde R, Oliveira N, Morais E, Amaral AP, Sousa A, Graca G, et al. NMR analysis seeking for cognitive decline and dementia metabolic markers in plasma from aged individuals. J Pharm Biomed Anal. 2024;238:115815. https://doi.org/10.1016/j.jpba.2023.115815
63. Andersen JV, Skotte NH, Christensen SK, Polli FS, Shabani M, Markussen KH, et al. Hippocampal disruptions of synaptic and astrocyte metabolism are primary events of early amyloid pathology in the 5xFAD mouse model of Alzheimer's disease. Cell Death Dis. 2021;12:954. https://doi.org/10.1038/s41419-021-04237-y
64. Pandey RS, Arnold M, Batra R, Krumsiek J, Kotredes KP, Garceau D, et al. Metabolomics profiling reveals distinct, sex-specific signatures in serum and brain metabolomes in mouse models of Alzheimer's disease. Alzheimers Dement. 2024;20:3987–4001. https://doi.org/10.1002/alz.13851
65. Mielke MM, Vemuri P, Rocca WA. Clinical epidemiology of Alzheimer's disease: assessing sex and gender differences. Clin Epidemiol. 2014;6:37–48. https://doi.org/10.2147/clep.s37929
66. Bundy JL, Vied C, Badger C, Nowakowski RS. Sex-biased hippocampal pathology in the 5XFAD mouse model of Alzheimer's disease: a multi-omic analysis. J Comp Neurol. 2019;527:462–75. https://doi.org/10.1002/cne.24551
67. Bouter C, Irwin C, Franke TN, Beindorff N, Bouter Y. Quantitative brain positron emission tomography in female 5XFAD Alzheimer mice: pathological features and sex-specific alterations. Front Med. 2021;8:745064. https://doi.org/10.3389/fmed.2021.745064
68. Zhang C, Zhang Y, Shen Y, Zhao G, Xie Z, Dong Y. Anesthesia/Surgery induces cognitive impairment in female Alzheimer's disease transgenic mice. J Alzheimers Dis. 2017;57:505–18. https://doi.org/10.3233/JAD-161268

ACKNOWLEDGEMENTS

We would like to thank the National Institutes of Health (NIH) for funding support (R01 grant numbers AG070257 and CA273010), as well as the Massachusetts General Hospital Athinoula A. Martinos Center for Biomedical Imaging. We would also like to thank the Canadian Institute of Health Research (CIHR) for the following postdoctoral training fellowship: MFE-194064. Authors FK, EJZ and RGB contributed equally.

AUTHOR CONTRIBUTIONS

FK: Methodology, Conceptualization, Data Acquisition, Data Analysis, Writing-Original Draft. EJZ: Methodology, Conceptualization, Data Acquisition, Formal Analysis, Visualization, Writing-Original Draft. RGB: Investigation, Formal Analysis, Visualization, Writing-Original Draft, Writing – Review & Editing. MK: Resources, Data Acquisition. JC: Resources, Software Design. JXZ: Resources, Software Design. AR: Resources, Software Design. JS: Data Analysis. XW: Resources, Data Analysis, Software design. WL: Sample Preparation. IHM: Resources, Sample Preparation. PH: Conceptualization, Supervision. JN: Conceptualization, Supervision. ZX: Conceptualization, Project Administration, Supervision, Writing – Review & Editing, Funding Acquisition. YZ: Conceptualization, Project Administration, Supervision, Writing – Review & Editing. LLC: Conceptualization, Project Administration, Supervision, Writing – Review & Editing, Funding Acquisition.

COMPETING INTERESTS

The authors declare no competing interests.

ADDITIONAL INFORMATION

Supplementary information The online version contains supplementary material available at https://doi.org/10.1038/s41398-025-03293-8.

Correspondence and requests for materials should be addressed to Yiying Zhang or Leo L. Cheng.

Reprints and permission information is available at http://www.nature.com/reprints

Publisher's note Springer Nature remains neutral with regard to jurisdictional claims in published maps and institutional affiliations.

QUERY FORM

TP	
Manuscript ID	**[Art. Id: 3293]**
Author	
Editor	
Publisher	

Journal: TP

Author :- The following queries have arisen during the editing of your manuscript. Please answer by making the requisite corrections directly in the e.proofing tool rather than marking them up on the PDF. This will ensure that your corrections are incorporated accurately and that your paper is published as quickly as possible.

Query No.	Description	Author's Response
GQ	Author surnames have been highlighted - please check these carefully and indicate if the first name or surname have been marked up incorrectly. Please note that this will affect indexing of your article, such as in PubMed.	